Tailoring Molecular Self-Assembly of Magnetic Phthalocyanine Molecules on Fe- and Co-Intercalated Graphene

Maciej Bazarnik,* Jens Brede,* Régis Decker, and Roland Wiesendanger

Institute of Applied Physics, University of Hamburg, Jungiusstrasse 11, D-20355 Hamburg, Germany

ABSTRACT We investigate molecule–molecule, as well as molecule–substrate, interactions of phthalocyanine molecules deposited on graphene. In particular, we show how to tune the self-assembly of molecular lattices in two dimensions by intercalation of transition metals between graphene and Ir(111): modifying the surface potential of the graphene layer via intercalation leads to the formation of square, honeycomb, or Kagome lattices. Finally, we demonstrate that such surface induced molecular lattices are stable even at room temperature.

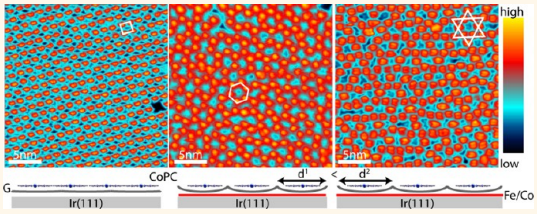

KEYWORDS: phthalocyanine · graphene · intercalation · scanning tunneling microscopy · template · surface engineering

The design of next generation electronics is driven by the necessity of ever faster, smaller, and more efficient components. In 1974, Aviram and Ratner proposed the use of organic molecules[1] instead of modern silicon based technology that would allow the miniaturization of electronic circuits down to the single molecule scale. Besides the reduction in size, usage of single molecules as isolated functional entities holds potential for a rational design by synthetic means, that is, either tailoring the molecule–molecule interactions by functionalizing individual molecules or tailoring the molecule–substrate interactions and taking advantage of molecular self-assembly processes. To this end, however, a detailed understanding of the interactions of these molecular building blocks among each other as well as with their surroundings is of utter importance. In particular, the electronic and conformational properties of molecules are known to undergo drastic changes when adsorbed directly on metal surfaces. Recently, graphene has emerged as a particularly promising template to study molecular self-assembly because it is known to be chemically inert and thus is believed to only slightly modify pristine molecular properties[2,3] while it allows driving of different, highly ordered macroscopic assemblies with nanoscale variations.[4,5] Moreover, recent advances in single molecule devices demonstrate the potential of crafting single-molecule magnets onto a carbon conductor, for example, to read out nuclear spin-states.[6]

Phthalocyanine (PC) molecules are particularly suitable for STM studies due to their robust nature that allows for thermal evaporation under UHV conditions, as well as their flat two-dimensional structure on surfaces already observed in pioneering STM experiments.[7,8] More recently, PC–metal contacts,[9,10] conformational changes,[11] adsorption-site-specific metal interactions,[12] site- and spin-dependent PC–ferromagnet interactions,[13,14] PC–superconductor interactions,[15,16] and site- and orbital-dependent electron doping[17–19] were demonstrated for single PC molecules. Moreover, tailoring reactivity and self-assembly of PCs was shown to produce switchable two-dimensional spin arrays.[20] These examples illustrate the versatility of this class of molecules for potential applications in molecular electronics. The growth and self-assembly of different PC molecules at monolayer and submonolayer coverage was studied predominantly on various metal surfaces[8,21,22] but also on semiconductor[23] and insulating thin film surfaces.[24] In most cases, the PC molecules lie flat on the surface and assemble into a densely packed square or rectangular pattern reflecting the 4-fold symmetry of the PC molecule itself, while different stages of the growth

* Address correspondence to mbazarni@physnet.uni-hamburg.de, jbrede@physnet.uni-hamburg.de.

Received for review October 7, 2013 and accepted November 26, 2013.

Published online November 26, 2013
10.1021/nn405172q

reflect the subtle differences between molecule–molecule and molecule–substrate interactions.

In this paper, we demonstrate how PC molecules adsorbed on a graphene layer can be driven into various two-dimensional lattices. In particular, we utilize graphene patches grown on an Ir(111) crystal, which can be tuned in size and orientation with respect to the underlying Ir(111) surface by appropriate growth conditions.[25] It is known that properties of graphene vary depending on the underlying metal substrate.[26,27] In order to unveil the changes in the self-assembly depending on the metal beneath the graphene, we exploit the intercalation of Fe or Co layers, motivated by the fact that a substantial geometric and electronic modulation on the nanometer scale can be induced by intercalation of different elements between the Ir(111) surface and the graphene layer.[28–31]

RESULTS AND DISCUSSION

Surface Potential. When graphene (G) grown on top of the Ir(111) surface is imaged with STM, it exhibits a characteristic Moiré pattern with a periodicity of ~2.5 nm due to the lattice mismatch of graphene and iridium.[25] Three distinct regions of the Moiré unit cell are commonly distinguished: top, fcc and hcp sites (see Figure 1a for an STM image with the different regions indicated and Figure 1d for a structure model). A Moiré pattern of similar lateral dimensions was recently reported for G/Fe/Ir(111) (see also Figure 1b), G/Co/Ir(111)[29] (Figure 1c), and G/Ni/Ir(111).[30] While the lateral dimensions are similar in all cases there are drastic differences in the corrugation dG (defined here as the difference in height of carbon atoms in the top-region compared with the valley regions, see also Figure 1e), which is ~3.5 pm for G/Ir while it is ~120–150 pm for G/Co/Ir, G/Ni/Ir, and G/Fe/Ir. The chemical environment of the carbon atoms leads to modifications of the electronic structure compared with free-standing graphene. The modifications are comparably weak for G/Ir, for example, the band structure of G/Ir(111) is very similar to free standing graphene,[32] while a strong hybridization of the graphene π-band with the transition metal is observed for G/Ni/Ir(111).[30] The strong hybridization of the graphene π-states with the metal d-states at the fcc and hcp sites leads to the formation of a nanometer-scale magnetic Moiré pattern for G/Co/Ir.[29] It was previously reported that surfaces that exhibit characteristic Moiré patterns with similar dimensions as the ones reported here exhibit two distinct properties that influence the adsorption of PC molecules. First, it was shown by Lin and Nilius that the local modulation of surface dipole moments leads to a selective adsorption of magnesium PC molecules, that is, the molecules are predominantly found at the fcc sites, when deposited on FeO on Pt(111).[33] More recently, Huang *et al.* demonstrated that chloroaluminium phthalocyanine (ClAlPC) molecules can

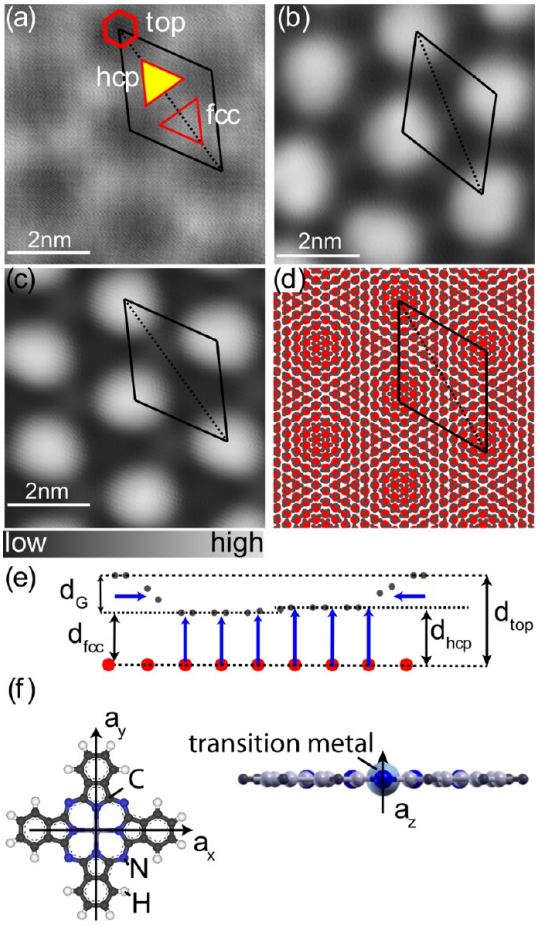

Figure 1. Surface potential and molecular structure. Typical STM images of Moiré patterns for (a) G/Ir, (b) G/Fe/Ir, (c) G/Co/Ir, and (d) a simple structure model (top view). Carbon atoms are dark gray and atoms of the top surface layer beneath graphene are indicated as red spheres. (e) Structure model (side view), following the dotted line indicated in panels a–d. Blue arrows indicate expected induced dipole moments. (f) Metal phthalocyanine (MPC) model (left, top view; right, side view). The different directions of the polarizability tensor a of a MPC are indicated.

be selectively trapped on the SiC nanomesh.[34] The depressions within the SiC nanomesh which make up a pore exhibit a significant out-of-plane dipole moment due to a charge transfer from the SiC to the topmost carbon layer. The charge transfer is greatly reduced (or absent) at the edge of the nanomesh where the C atoms are further away from the SiC, thus a nanoscale modulation of out-of-plane dipole moments across the SiC nanomesh is induced. The energetically most favorable alignment of the permanent molecular dipole of the ClAlPC molecules with respect to the surface dipole moments drives the molecular assembly. Interestingly, Chen *et al.* demonstrated that planar CuPC molecules, which lack an axial ligand (and therefore a permanent dipole moment), also assemble in ordered arrays that follow the symmetry of the SiC nanomesh.[35] A modulation of out-of-plane surface dipole moments can also be expected for the graphene surfaces investigated here. Atoms within the Moiré cell that are in strong chemical interaction, that is, the fcc and hcp regions, will

experience a charge rearrangement between the metal surface and the carbon atoms. In particular, the carbon sp^2 states will be partially driven into a sp^3 configuration owing to the hybridization with the metal surface. This effect is absent or greatly reduced at the top sites due to the large graphene−substrate distance; here, the interactions between carbon and metal atoms are of van der Waals (VdW) type. Thus, surface dipole moments that vary across the Moiré cell are formed. Second, the strain induced in the graphene layer due to the local corrugation leads to the formation of considerable in-plane dipole moments that can lead to trapping of PC molecules due to their in-plane polarizability.[36,37] In Figure 1e, we schematically depict the different regions of the graphene layer on top of the metal surfaces, and the resulting dipole moments are indicated. The in-plane polarizability of metal PC molecules is an order of magnitude larger than the out-of-plane polarizability and depends only slightly on the central metal atom.[38] Nonetheless, Yang *et al.* found a distinct influence of the central molecular metal atom on the self-assembly of MPC molecules when deposited on G/Ru(0001).[39] In order to understand the surface potential of G/Co/Ir(111) and G/Fe/Ir(111) and its influence on molecular self-assembly, we study, in a first step, the growth of cobalt phthalocyanine (CoPC) molecules at low temperatures. When molecules are deposited on a precooled substrate, surface diffusion is quickly frozen and metastable adsorption sites may be observed.[40] Thus, a detailed understanding of the surface induced restrictions on molecular assembly can be gained.

Cobalt Phthalocyanine Growth on Precooled Graphene. The self-assembly of CoPC molecules on Co or Fe intercalated graphene on Ir, which was held at low temperature (∼35 K) during molecule deposition, is depicted in Figure 2. At a dilute CoPC coverage of ∼0.01 ML (a coverage of one monolayer is defined as the almost square lattice with a periodicity of 1.4 nm as observed for CoPC on G/Ir(111) Figure 3b), the uncovered G/Co/Ir (Figure 2a) or G/Fe/Ir (Figure 2b) surface is easily identified by the respective Moiré pattern as introduced above: the top sites (blue−red) appear as topographic protrusions, the fcc and hcp sites (dark blue−light blue) as valleys. Individual CoPC molecules appear as topographic maxima (red−yellow). The molecules are situated either at hcp sites (inset, Figure 2a, top right) or fcc sites (inset, Figure 2a, middle right; Figure 2b, top right) and either are isolated surface monomers[41] or form surface dimers (*e.g.*, see inset, Figure 2b, middle right, and inset of Figure 2c, middle right). The direct comparison of the molecular growth on both surfaces shows that surface monomers occupy predominantly fcc sites but also hcp sites on G/Co/Ir, while they are exclusively situated at fcc sites on G/Fe/Ir. Thus, the local energy minimum for surface monomers on both surfaces is the fcc site, while the hcp site is only a metastable adsorption site on G/Co/Ir. Furthermore, there are almost as many surface dimers as surface monomers on G/Fe/Ir while more than 80% of CoPC molecules are surface monomers on G/Co/Ir. The ratio of molecules in fcc sites to molecules in hcp sites is ∼2.8:1 for G/Fe/Ir and ∼2.3:1 for G/Co/Ir, respectively.

At a higher coverage of 0.04 ML (Figure 2c) or 0.06 ML (Figure 2d), CoPC molecules start to form quasi one-dimensional chains. Surface trimers (see Figure 2d, top right) and surface polymers (*e.g.*, see inset Figure 2c, bottom right, and inset Figure 2d, middle right), that is, molecular assemblies of four or more molecules, are distinguished, and second layer molecules (inset Figure 2d, middle top) start to appear. Interestingly, most molecules on G/Co/Ir are still surface monomers, while almost 90% of all molecules on G/Fe/Ir form surface dimers, surface trimers, and surface polymers. The ratio of molecules in fcc vs hcp sites at this coverage is 1.8:1 for G/Co/Ir and 1.3:1 for G/Fe/Ir, respectively.

When the CoPC coverage is increased further to 0.15 ML for G/Co/Ir (Figure 2e) and 0.2 ML for G/Fe/Ir (Figure 2f), respectively, even longer chains and additional second layer molecules are observed, and quasi two-dimensional structures are formed predominantly where one-dimensional chains intersect. Particularly noteworthy are two-dimensional assemblies due to six CoPC situated in the valley sites around a top site (inset Figure 2e, top right, and inset Figure 2f, top right). This assembly may be extended to a two-dimensional honeycomb lattice. At these coverages, very few molecules are still found as surface monomers, and the ratio of fcc to hcp site molecules is ∼1.5:1 on both surfaces.

In summary, our low-temperature growth study shows that the top sites of both intercalated G/Ir surfaces are not (meta)stable adsorption sites for CoPC molecules because they remain strictly uncovered for all coverages studied. Furthermore, there is a slight difference for the valley sites, that is, between fcc and hcp sites for G/Co/Ir and G/Fe/Ir, respectively; this difference leads to the emergence of the hcp sites of G/Co/Ir as a metastable adsorption site for CoPC surface monomers. When molecules start to interact into surface dimers, surface trimers, and surface polymers, they form primarily one-dimensional chains. Two-dimensional assemblies form where chains intersect. CoPC molecules on G/Fe/Ir start assembling in chains at lower coverage than for CoPC on G/Co/Ir as manifested by the very rapid decline of surface monomers with increasing coverage for G/Fe/Ir compared with G/Co/Ir.

After addressing the restrictions on the molecular self-assembly at low temperatures, we will turn now to analyze molecular assemblies that are formed when the samples are warmed to or kept at room temperature (RT) during molecule deposition. Molecules deposited onto these samples have sufficient thermal energy to reach their thermal equilibrium distribution.

Surface Engineered Molecular Lattices. We observe that submonolayer coverage of CoPC molecules self-assemble on graphene on Ir(111) at room temperature in an almost square lattice with lattice vectors of ∼1.4 nm

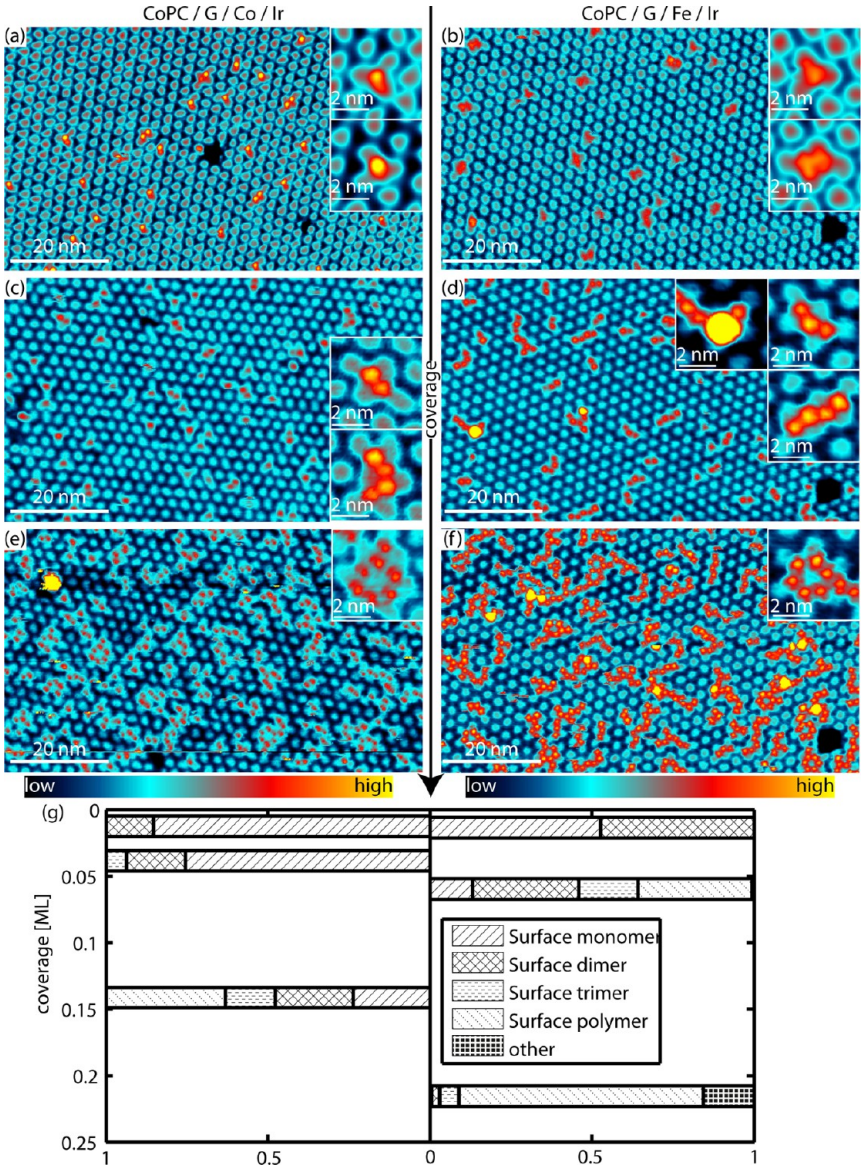

Figure 2. Low temperature growth of CoPC molecules on Co (a, c, e) and Fe (b, d, f) intercalated graphene. Insets show in panel a CoPC surface monomers in either hcp (top right) or fcc (middle right) adsorption sites, in panel b a CoPC surface monomer at the fcc site (top right) and a CoPC surface dimer (middle right), in panel c a CoPC surface dimer (middle right) and a chain-like surface polymer (bottom right), in panel d a second layer molecule on-top of a first layer surface polymer (top middle), a CoPC surface trimer (top right), and a chain-like surface polymer (middle right), in panel e a two-dimensional surface polymer (top right), and in panel f a two-dimensional surface polymer. In panel g, the relative occurrence of molecular assemblies following the nomenclature introduced above for different CoPC coverages is given.

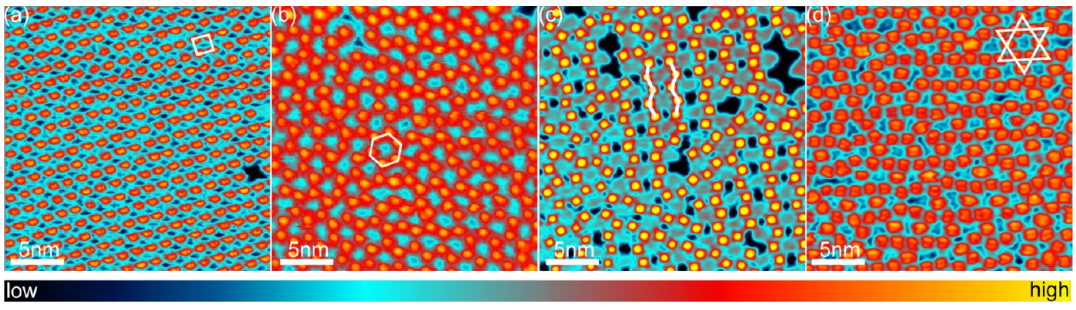

Figure 3. Different CoPC lattices on graphene: A square lattice on G/Ir(111) (a), a honeycomb lattice on G/Co/Ir(111) (b), a distorted honeycomb lattice on G/Fe/Ir(111) (c), and a Kagome lattice on a rotated G/Co/Ir(111) domain (d).

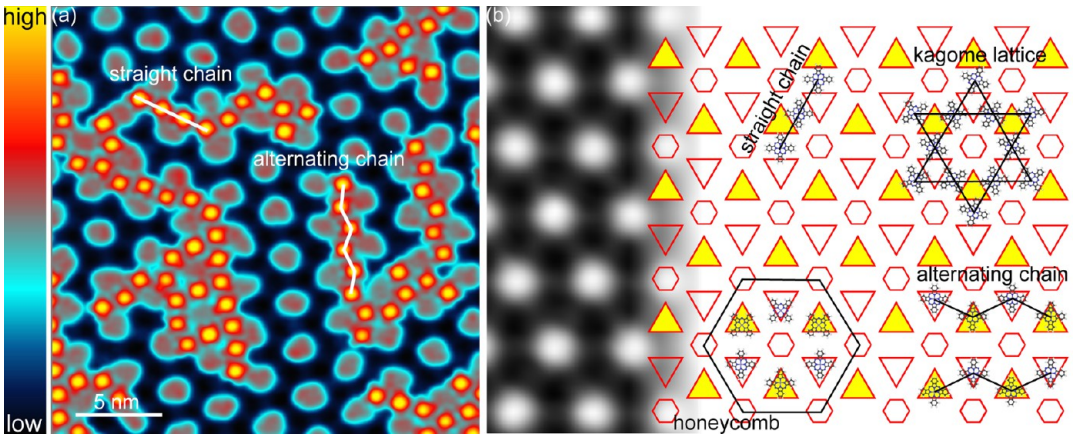

Figure 4. Molecular chains and assemblies. (a) High resolution image of 0.25 ML of CoPC molecules on G/Fe/Ir(111). Two different types of molecular chains are indicated. (b) Two-dimensional model geometry of the Moiré pattern of G/Fe/Ir as deduced from the STM image (background) is given by full (fcc) and empty (hcp) triangles, as well as the hexagons (top). The various model geometries of different molecular assemblies are illustrated with ball and stick models (see text for details).

(see Figure 3a), which is in agreement with a previous study by Hämäläinen *et al.*[4] Formation of a square molecular lattice on top of the hexagonal graphene lattice shows that molecule−substrate interactions are very weak and that molecule−molecule interactions dominate. Upon intercalation of Fe or Co, we observe slightly distorted honeycomb lattices (see Figure 3b,c), which correspond to a packed molecular lattice with the restrictions imposed by the surface potential as discussed above. In an attempt to further control the self-assembly into different molecular surface lattices, we took advantage of different rotational domains of the graphene lattice, which are known to appear when grown on top of the Ir(111) surface under appropriate conditions.[25] The rotation of the graphene lattice with respect to the underlying Ir(111) surface leads to Moiré patterns with a different periodicity compared with the unrotated case. The different rotational graphene domains are intercalated in a similar manner and form G/Fe/Ir (or G/Co/Ir) Moiré patterns that differ in periodicity. When the periodicity is in the range of 2.6−2.8 nm, we observe a distortion ("slits") of the honeycombe lattice (see Figure 3c). Using an appropriate periodicity of 2.85 nm, the molecular assembly can be tuned into a slightly distorted Kagome lattice (see Figure 3d and Figure 6d), similar to the one observed for phthalocyanine molecules on G/Ru(0001) where the periodicity of the surface Moiré pattern is ∼3 nm.

In order to identify the origin of the disorder in the molecular lattices, we studied high resolution images (Figure 4a) at low temperatures of a sample with a slightly lower coverage.

The high image resolution allows the deduction of model geometries for different molecular chains observed (Figure 4b). We can distinguish two different types of chains, namely, straight or alternating. The next-nearest neighbor distance is ∼2.7 nm for straight chains and ∼2.6 nm for alternating chains. In straight chains molecules are situated between fcc and hcp areas of the G/Fe/Ir Moiré cell, while in the case of alternating chains, all molecules populate fcc and hcp sites. Neighboring molecules of all chain types follow a distinct directionality. That is the outer C−H group of one molecule tries to align with the outer N of the next. While this directionality is typical for the formation of a hydrogen bond, it is clear that in the present case the H−N distance of more than 500 pm is too large to be considered a hydrogen bond.[42,43] Therefore, the molecule−molecule interactions are either of electrostatic or VdW type. Note that with increasing coverage the formation of alternating chains is preferred over the formation of straight chains (compare Figure 3, panels b and c). This is readily understood as the alternating chains allow for a denser packing of the first molecular layer. When two alternating chains are parallel, they may form a local honeycomb structure by rotating the molecules in one of the chains (as depicted in the model) but usually they remain in their alternating chain structure, which leads to the formation of characteristic "slits" in the STM images (see Figure 3c). The formation of the "slit", as well as the local honeycomb structure, can again be understood when the directionality of the intermolecular bonding is considered. It is only favorable when C−H bonds align with an outer N of the next molecule; therefore, molecules in one of the two parallel alternating chains rotate by 45° when the lateral separation of two chains is reduced. As introduced above, for particular rotational domains of graphene with respect to the underlying Ir(111) surface, a Moiré pattern that exhibits a slightly larger periodicity of 2.85 nm is observed, and in this case molecules form a Kagome lattice (see Figure 4b, top right, for the model depiction and Figure 3d for the STM image). Here, all molecules are adsorbed between fcc and hcp regions and the rotational orientation of each molecule maximizes the H−C to N interactions with its four nearest neighbors. Note that the Kagome lattice exhibits a 3-fold structure, while the CoPC molecule is strictly 4-fold; therefore the

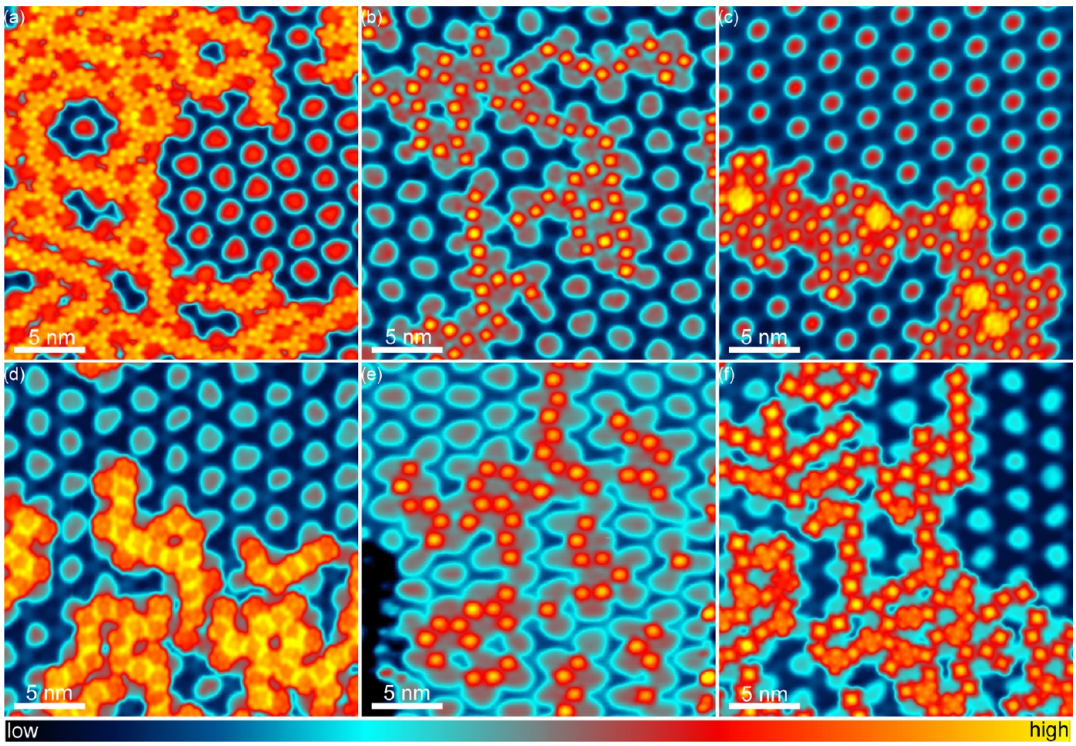

Figure 5. Different assemblies studied: (a) CuPC on G/Fe/Ir(111), (b) CoPC on G/Fe/Ir(111), (c) mixture of CuPC and CoPC on G/Fe/Ir(111), (d) CuPC on G/Co/Ir(111), (e) CoPC on G/Co/Ir(111), and (f) mixture of CuPC and CoPC on G/Co/Ir(111).

formation of a commensurate molecular lattice on top of the surface is not possible. Kagome lattices are an example of magnetically frustrated systems. The fact that we can obtain a Kagome structure built with magnetic molecules is of considerable importance for future studies of magnetic coupling phenomena in these kind of systems.

In order to get more insight into the delicate balance of molecule−molecule, as well as molecule−substrate, interactions during the formation of the different lattices, we performed a direct comparison of cobalt phthalocyanine with copper phthalocyanine (CuPC) molecules deposited on both G/Fe/Ir and G/Co/Ir.

Influence of the Metal Center on the Molecular Assembly. To address a possible influence of the central metal atom within PC molecules on their self-assembly, we studied both CuPC and CoPC on Co and Fe intercalated G/Ir. The molecule deposition was performed with the substrate held at room temperature before cooling them to the measurement temperature of 6.5 K. Figure 5 shows STM images of different preparations imaged with different tips and different tunneling conditions. CuPC and CoPC molecules can easily be distinguished by their appearance in the STM images, in particular, CoPC molecules always show a profound central maximum whereas CuPC molecules do not.[44] In all cases, the self-assemblies appear similar. Straight and alternating chains, as well as local honeycomb and local Kagome lattices, are readily identified in all preparations. The details of the molecular assembly, that is, chain length, number of two-dimensional networks, *etc.*, is strictly determined by the local coverage and is independent of the choice of the central metal atom. Differences between the Co and Fe intercalated G/Ir surfaces diminish when the diffusion barrier is thermally overcome during the deposition onto a substrate held at RT. In all studied systems, three main factors remain important, namely, substrate temperature during deposition, (local) coverage, and the periodicity of the underlying surface Moiré pattern.

We note that a rotation of the graphene lattice with respect to the underlying surface not only changes the periodicity of the observed Moiré pattern but also alters the local chemical environment of the C atoms. As discussed above, this will have a significant influence on the chemical properties of the C atoms. It is also noted that employing different rotational domains of G/Ir is accompanied by a much smaller domain size of the different graphene patches. Thus, edge and confinement effects become more important. Moreover a change of the geometry of the top sites of the G/Co (or Fe)/Ir Moiré pattern from circular to 6- or 3-fold is expected to have substantial influence on the self-assembly due to subtle changes in the surface potential. Up to now, we did not see a correlation of the appearance of the top sites in STM images with the preference of the formation of a particular molecular lattice. Figure 5 clearly illustrates how the appearance of the top sites of the G/Fe/Ir and G/Co/Ir surfaces can undergo subtle

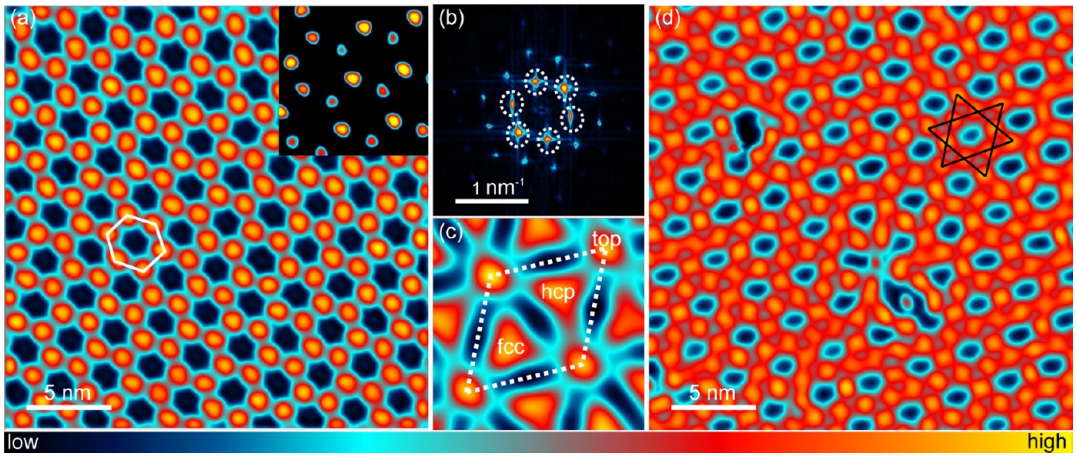

Figure 6. Thermal stability of CoPC on G/Fe/Ir and G/Co/Ir. (a) STM image of G/Fe/Ir taken at RT. Inset in panel a shows part of the molecular assembly in a saturated color scale revealing a height-modulation, that is, two triangular lattices, one consisting of higher and one of lower appearing molecules. The Fourier transformation of panel a is shown in panel b: first order spots of the hexagonal lattice are marked by the dashed circles. Panel c shows the FFT filtered image with the hexagonal lattice suppressed, in order to highlight the fcc, hcp, and top regions of the Moiré. Kagome lattice of CoPC/G/Co/Ir imaged at RT is shown in panel d. A larger periodicity of the uncovered top sites (dark blue) of the underlying G layer compared with panel a is apparent.

variations but the observed molecular lattices remain essentially the same.

Thermal Stability. For all application purposes, thermal stability is of utter importance. In order to address this aspect, an STM image of CoPC molecules on G/Fe/Ir(111) taken at 300 K is shown in Figure 6a. A highly regular honeycomb lattice with a periodicity of 2.7 nm is clearly visible. Interestingly the two triangular sublattices of the honeycomb lattice can clearly be distinguished [see inset of Figure 6a]. The uncovered top sites of the G/Fe/Ir Moiré pattern (dark blue) appear strictly hexagonal. In order to gain further insight into the highly regular pattern observed, we analyzed the Fourier transform (Figure 3b). Besides the first order spots of the honeycomb lattice (marked by circles) higher-order spots are clearly present. We visualize the substructure by suppressing ("band-cut") the first order spots and performing an inverse Fourier transform. The resulting Fourier-filtered real space image is shown in Figure 6c: a round protrusion is clearly visible at the central position of the top sites and two triangular protrusions separated by broad lines at the fcc sites and hcp sites. The overall symmetry of the image is strongly reminiscent of the uncovered G/Fe/Ir Moiré pattern (compare Figure 1b).

We interpret the observed patterns in terms of the two following effects: first, the protrusions observed in Figure 6a arise due to the contribution of the CoPC molecule's d_{z^2} orbital to the tunneling current, which normally leads to a circular protrusion.[44] Second, the molecules are not static at the given temperature but diffuse around their lattice sites while confined by the surface potential and molecule–molecule interactions. The diffusion (much faster than the scan speed) around the fcc/hcp sites of the underlying G/Fe/Ir(111) Moiré leads to the triangular distortion of the protrusions observed in Figure 6a (best visualized in the FFT filtered image in Figure 6c).The Kagome lattice that is observed for larger Moiré periodicity also shows stability at room temperature as illustrated in Figure 6d.

Remarkably, although the exact positions of molecules might be blurred, the self-assembly itself is stable even at room temperature. This demonstrates that such weakly bound molecular surface lattices can even be maintained at elevated temperatures making them interesting for application oriented studies.

CONCLUSIONS

We studied the assemblies of different metal–phthalocyanine molecules on different graphene-based templates. In agreement with previous results, we found that at submonolayer coverage, PC molecules on G/Ir(111) form an almost square lattice due to weak molecule–surface interactions. We tailored the molecular self-assembly by intercalating Co and Fe between graphene and Ir. The Fe or Co intercalated G/Ir surfaces exhibit a Moiré pattern with a similar periodicity as G/Ir but with a much higher corrugation. The surface potential for molecular adsorption is completely altered for the intercalated systems compared with the bare G/Ir. In particular, the top sites of the Moiré pattern remain strictly uncovered. This restriction for the molecular assembly leads at very low coverages primarily to a one-dimensional growth of molecular chains for both CoPC and CuPC molecules on G/Fe/Ir(111) as well as G/Co/Ir(111). Different types of molecular chains are shown to coexist on the same surface. With increasing coverage, a honeycomb lattice is formed where molecular chains intersect. The two-dimensional molecular surface lattice can be further tuned by exploiting surface Moiré patterns with different periodicities. When the periodicity is increased from 2.5 to 3 nm, a transition from a honeycomb to a Kagome lattice can be induced. These surface potential driven molecular lattices rely on molecule–surface interactions rather than on molecule–molecule

interactions; therefore, it is expected that such ordered lattices will disintegrate when the sample temperature is increased and molecular diffusion sets in. Nonetheless, we could clearly demonstrate the stability of ordered honeycomb and Kagome lattices up to room temperature. The different self-assembled magnetic molecule lattices may open a route to study magnetic frustration as a function of lattice size and symmetry, interaction effects, and individual molecules magnetic properties.

METHODS

All experiments were performed in two UHV systems equipped with either a low temperature STM or a variable temperature STM and preparation chambers for substrate cleaning, CVD growth, and molecule, as well as metal, deposition. Electrochemically etched tungsten tips were used as STM probes and cleaned by standard procedures. The Ir(111) crystals were cleaned by repeated cycles of Ar^+ sputtering (1 kV, 5×10^{-6} mbar), oxygen annealing (ramp 600 to 1400 K, $pO_2 = 1 \times 10^{-7}$ mbar), and a final "flash" heating (1470 K). Surface quality was directly assured by STM. Graphene was grown *in situ* on top of the clean Ir via ethylene cracking following the procedure outlined in ref 45. Intercalation of Co or Fe between graphene and the Ir surface was performed *in situ* following the method described elsewhere.[29] Molecules were deposited from thoroughly outgassed sources by thermal evaporation under UHV conditions either onto the precooled sample directly into the STM or onto the sample held at room temperature in the preparation chamber (in the latter case, the sample was given sufficient time (30−60 min) to reach thermal equilibrium). Finally, samples were transferred (if necessary) *in vacuo* to the STM and cooled to measurement temperatures. All images were recorded in constant current mode and processed using the WSxM software.[46]

Image parameter: Figure 1, (a) −1.1 V/z:[0; 16]pm, $T = 6.5$ K, (b) 2.5 nA/0.5 V/z:[0; 142]pm $T = 6.5$ K, (c) −1.1 V/z:[0; 170]pm, $T = 6.5$ K; Figure 2, (a) 10 pA/1.5 V/z:[0; 300]pm, inset [0; 150]pm, (b) 10 pA/1.5 V/z:[0; 200]pm, inset [0; 150]pm, (c) 3pA/1.5 V/z:[0; 300]pm, inset [0; 200]pm, (d) 3 pA/1.5 V/z:[0; 300]pm, inset [0; 200]pm, (e) 10 pA/1.5 V/z:[0; 300]pm, (f)10 pA/1.5 V/z:[0; 300]pm; Figure 3, (a) 100 pA/1 V/z:[0; 461]pm, (b) 10 pA/−1 V/z:[0; 330]pm, (c) 100 pA/0.25 V/z:[0;179]pm, and (d) 10 pA/0.5 V/z:[0; 408]pm; Figure 4, 100 pA/0.25 V/z:[0; 260]pm; Figure 5, (a) 100 pA/−0.5 V/z:[0; 211]pm, (b) 100 pA/0.25 V/z:[0; 303]pm, (c) 100pA/0.75 V/z:[0; 280]pm, (d) 100pA/0.5 V/z:[0; 266]pm, (e) 100pA/0.5 V/z:[0; 305]pm, and (f) 100pA/0.75 V/z:[0; 306]pm. Figure 6 (a): 75pA/-2.5 V/z:[0; 143]pm, $T = 300$ K, inset z:[0; 251]pm, $T = 300$ K; (d) 10 pA/−1 V/z:[0; 422]pm.

Conflict of Interest: The authors declare no competing financial interest.

Acknowledgment. We gratefully acknowledge financial support from the ERC Advanced Grant FURORE and the DFG via SFB668. J.B. is grateful for fruitful discussions with Nicolae Atodiresei.

REFERENCES AND NOTES

1. Aviram, A.; Ratner, M. Molecular Rectifiers. *Chem. Phys. Lett.* **1974**, *29*, 277.
2. Lei, S.; Feng, W.; Li, B.; Li, Q.; Zhao, A.; Wang, B.; Yang, J.; Hou, J. G. Orbital-Selective Single Molecule Rectifier on Graphene-Covered Ru(0001) Surface. *Appl. Phys. Lett.* **2013**, *102*, No. 163506.
3. Järvinen, P.; Hämäläinen, S. K.; Banerjee, K.; Häkkinen, P.; Ijäs, M.; Harju, A.; Liljeroth, P. Molecular Self-Assembly on Graphene on SiO_2 and h-BN Substrates. *Nano Lett.* **2013**, *13*, 3199–3204.
4. Hämäläinen, S. K.; Stepanova, M.; Drost, R.; Liljeroth, P.; Lahtinen, J.; Sainio, J. Self-Assembly of Cobalt-Phthalocyanine Molecules on Epitaxial Graphene on Ir(111). *J. Phys. Chem. C* **2012**, *116*, 20433–20437.
5. Mao, J.; Zhang, H.; Jiang, Y.; Pan, Y.; Gao, M.; Xiao, W.; Gao, H.-J. Tunability of Supramolecular Kagome Rattices of Magnetic Phthalocyanines Using Graphene-Based Moire Patterns as Templates. *J. Am. Chem. Soc.* **2009**, *131*, 14136–14137.
6. Vincent, R.; Klyatskaya, S.; Ruben, M.; Wernsdorfer, W.; Balestro, F. Electronic Read-Out of a Single Nuclear Spin Using a Molecular Spin Transistor. *Nature* **2012**, *488*, 357–360.
7. Gimzewski, J.; Stoll, E.; Schlittler, R. Scanning Tunneling Microscopy of Individual Molecules of Copper Phthalocyanine Adsorbed on Polycrystalline Silver Surfaces. *Surf. Sci.* **1987**, *181*, 267–277.
8. Lippel, P.; Wilson, R.; Miller, M.; Woll, C.; Chiang, S. High-Resolution Imaging of Copper-Phthalocyanine by Scanning-Tunneling Microscopy. *Phys. Rev. Lett.* **1989**, *62*, 171.
9. Nazin, G. V.; Qiu, X. H.; Ho, W. Visualization and Spectroscopy of a Metal-Molecule-Metal Bridge. *Science* **2003**, *302*, 77–81.
10. Schmaus, S.; Bagrets, A.; Nahas, Y.; Yamada, T. K.; Bork, A.; Bowen, M.; Beaurepaire, E.; Evers, F.; Wulfhekel, W. Giant Magnetoresistance through a Single Molecule. *Nat. Nanotechnol.* **2011**, *6*, 185–189.
11. Zhao, A.; Li, Q.; Chen, L.; Xiang, H.; Wang, W.; Pan, S.; Wang, B.; Xiao, X.; Yang, J.; Hou, J. G.; *et al.* Controlling the Kondo Effect of an Adsorbed Magnetic Ion Through Its Chemical Bonding. *Science* **2005**, *309*, 1542–1544.
12. Gao, L.; Ji, W.; Hu, Y. B.; Cheng, Z. H.; Deng, Z. T.; Liu, Q.; Jiang, N.; Lin, X.; Guo, W.; Du, S. X.; *et al.* Site-Specific Kondo Effect at Ambient Temperatures in Iron-Based Molecules. *Phys. Rev. Lett.* **2007**, *99*, No. 106402.
13. Iacovita, C.; Rastei, M.; Heinrich, B.; Brumme, T.; Kortus, J.; Limot, L.; Bucher, J. Visualizing the Spin of Individual Cobalt-Phthalocyanine Molecules. *Phys. Rev. Lett.* **2008**, *101*, No. 116602.
14. Brede, J.; Atodiresei, N.; Kuck, S.; Lazić, P.; Caciuc, V.; Morikawa, Y.; Hoffmann, G.; Blügel, S.; Wiesendanger, R. Spin- and Energy-Dependent Tunneling through a Single Molecule with Intramolecular Spatial Resolution. *Phys. Rev. Lett.* **2010**, *105*, No. 047204.
15. Franke, K. J.; Schulze, G.; Pascual, J. I. Competition of Superconducting Phenomena and Kondo Screening at the Nanoscale. *Science* **2011**, *332*, 940–944.
16. Fu, Y.-S.; Ji, S.-H.; Chen, X.; Ma, X.-C.; Wu, R.; Wang, C.-C.; Duan, W.-H.; Qiu, X.-H.; Sun, B.; Zhang, P.; *et al.* Manipulating the Kondo Resonance through Quantum Size Effects. *Phys. Rev. Lett.* **2007**, *99*, No. 256601.
17. Swart, I.; Sonnleitner, T.; Repp, J. Charge State Control of Molecules Reveals Modification of the Tunneling Barrier with Intramolecular Contrast. *Nano Lett.* **2011**, *11*, 1580–1584.
18. Robles, R.; Lorente, N.; Isshiki, H.; Liu, J.; Katoh, K.; Breedlove, B. K.; Yamashita, M.; Komeda, T. Spin Doping of Individual Molecules by Using Single-Atom Manipulation. *Nano Lett.* **2012**, *12*, 3609–3612.
19. Krull, C.; Robles, R.; Mugarza, A.; Gambardella, P. Site- and Orbital-Dependent Charge Donation and Spin Manipulation in Electron-Doped Metal Phthalocyanines. *Nat. Mater.* **2013**, *12*, 337–343.
20. Wäckerlin, C.; Nowakowski, J.; Liu, S.-X.; Jaggi, M.; Siewert, D.; Girovsky, J.; Shchyrba, A.; Hälen, T.; Kleibert, A.; Oppeneer, P. M.; *et al.* Two-Dimensional Supramolecular Electron Spin Arrays. *Adv. Mater.* **2013**, *25*, 2404–2408.
21. Dufour, G.; Poncey, C.; Rochet, F.; Roulet, H.; Iacobucci, S.; Sacchi, M.; Yubero, F.; Motta, N.; Piancastelli, M. N.; Sgarlata, A.; *et al.* Metal Phthalocyanines (MPc, M=Ni, Cu) on Cu (001) and Si (001) Surfaces Studied by XPS, XAS and STM. *J. Electron Spectrosc. Relat. Phenom.* **1995**, *76*, 219–224.

22. Qiu, X.; Wang, C.; Zeng, Q.; Xu, B.; Yin, S.; Wang, H.; Xu, S.; Bai, C. Alkane-Assisted Adsorption and Assembly of Phthalocyanines and Porphyrins. *J. Am. Chem. Soc.* **2000**, *122*, 5550–5556.
23. Yim, S.; Jones, T. Structure of Phthalocyanine Overlayers on the (100) Surfaces of InSb and InAs. *Surf. Sci.* **2002**, *521*, 151–159.
24. Wang, Y.; Kröger, J.; Berndt, R.; Tang, H. Molecular Nanocrystals on Ultrathin NaCl Films on Au(111). *J. Am. Chem. Soc.* **2010**, *132*, 12546–12547.
25. T N'Diaye, A.; Engler, M.; Busse, C.; Wall, D.; Buckanie, N.; Meyer zu Heringdorf, F.-J.; van Gastel, R.; Poelsema, B.; Michely, T. Growth of Graphene on Ir(111). *New J. Phys.* **2009**, *11*, No. 023006.
26. Vinogradov, N. A.; Zakharov, A. A.; Kocevski, V.; Rusz, J.; Simonov, K. A.; Eriksson, O.; Mikkelsen, A.; Lundgren, E.; Vinogradov, A. S.; Mårtensson, N.; *et al.* Formation and Structure of Graphene Waves on Fe(110). *Phys. Rev. Lett.* **2012**, *109*, No. 026101.
27. Wintterlin, J.; Bocquet, M.-L. Graphene on Metal Surfaces. *Surf. Sci.* **2009**, *603*, 1841–1852.
28. Gråsäs, E.; Knudsen, J.; Schröder, U. A.; Gerber, T.; Busse, C.; Arman, M. A.; Schulte, K.; Andersen, J. N.; Michely, T. Oxygen Intercalation under Graphene on Ir(111): Energetics, Kinetics, and the Role of Graphene Edges. *ACS Nano* **2012**, *6*, 9951–9963.
29. Decker, R.; Brede, J.; Atodiresei, N.; Caciuc, V.; Blügel, S.; Wiesendanger, R. Atomic-Scale Magnetism of Cobalt-Intercalated Graphene. *Phys. Rev. B* **2013**, *87*, No. 041403.
30. Pacilé, D.; Leicht, P.; Papagno, M.; Sheverdyaeva, P. M.; Moras, P.; Carbone, C.; Krausert, K.; Zielke, L.; Fonin, M.; Dedkov, Y. S.; *et al.* Artificially Lattice-Mismatched Graphene/Metal Interface: Graphene/Ni/Ir(111). *Phys. Rev. B* **2013**, *87*, No. 035420.
31. Schumacher, S.; Förster, D. F.; Rösner, M.; Wehling, T. O.; Michely, T. Strain in Epitaxial Graphene Visualized by Intercalation. *Phys. Rev. Lett.* **2013**, *110*, No. 086111.
32. Pletikosić, I.; Kralj, M.; Pervan, P.; Brako, R.; Coraux, J.; N'Diaye, A.; Busse, C.; Michely, T. Dirac Cones and Minigaps for Graphene on Ir(111). *Phys. Rev. Lett.* **2009**, *102*, No. 056808.
33. Lin, X.; Nilius, N. Self-Assembly of MgPc Molecules on Polar FeO Thin Films. *J. Phys. Chem. C* **2008**, *112*, 15325–15328.
34. Huang, H.; Wong, S. L.; Sun, J.; Chen, W.; Wee, A. T. S. Trapping Single Polar Molecules in SiC Nanomesh via Out-of-Plane Dipoles. *ACS Nano* **2012**, *6*, 2774–2778.
35. Shi, C.; Wei, C.; Han, H.; Xingyu, G.; Dongchen, Q.; Yuzhan, W.; Wee, A. T. S. Template-Directed Molecular Assembly on Silicon Carbide Nanomesh: Comparison Between CuPc and Pentacene. *ACS Nano* **2010**, *4*, 849–854.
36. Dil, H.; Lobo-Checa, J.; Laskowski, R.; Blaha, P.; Berner, S.; Osterwalder, J.; Greber, T. Surface Trapping of Atoms and Molecules with Dipole Rings. *Science* **2008**, *319*, 1824–1826.
37. Zhang, H. G.; Sun, J. T.; Low, T.; Zhang, L. Z.; Pan, Y.; Liu, Q.; Mao, J. H.; Zhou, H. T.; Guo, H. M.; Du, S. X.; *et al.* Assembly of Iron Phthalocyanine and Pentacene Molecules on a Graphene Monolayer Grown on Ru(0001). *Phys. Rev. B* **2011**, *84*, No. 245436.
38. Ramprasad, R.; Shi, N. Polarizability of Phthalocyanine Based Molecular Systems: A First-Principles Electronic Structure Study. *Appl. Phys. Lett.* **2006**, *88*, No. 222903.
39. Yang, K.; Xiao, W. D.; Jiang, Y. H.; Zhang, H. G.; Liu, L. W.; Mao, J. H.; Zhou, H. T.; Du, S. X.; Gao, H.-J. Molecule-Substrate Coupling between Metal Phthalocyanines and Epitaxial Graphene Grown on Ru(0001) and Pt(111). *J. Phys. Chem. C* **2012**, *116*, 14052–14056.
40. Chang, S.-H.; Kuck, S.; Brede, J.; Lichtenstein, L.; Hoffmann, G.; Wiesendanger, R. Symmetry Reduction of Metal Phthalocyanines on Metals. *Phys. Rev. B* **2008**, *78*, No. 233409.
41. Pollino, J. M.; Weck, M. Non-Covalent Side-Chain Polymers: Design Principles, Functionalization Strategies, and Perspectives. *Chem. Soc. Rev.* **2005**, *34*, 193–207.
42. Arunan, E.; Desiraju, G. R.; Klein, R. A.; Sadlej, J.; Scheiner, S.; Alkorta, I.; Clary, D. C.; Crabtree, R. H.; Dannenberg, J. J.; Hobza, P.; *et al.* Defining the Hydrogen Bond: An account (IUPAC Technical Report). *Pure Appl. Chem.* **2011**, *83*, 1619–1636.
43. Barth, J. Molecular Architectonic on Metal Surfaces. *Annu. Rev. Phys. Chem.* **2007**, *58*, 375–407.
44. Hipps, K.; Lu, X.; Wang, X.; Mazur, U. Metal d-Orbital Occupation-Dependent Images in the Scanning Tunneling Microscopy of Metal Phthalocyanines. *J. Phys. Chem.* **1996**, *100*, 11207–11210.
45. N'Diaye, A. T.; Coraux, J.; Plasa, T. N.; Busse, C.; Michely, T. Structure of Epitaxial Graphene on Ir(111). *New J. Phys.* **2008**, *10*, No. 043033.
46. Horcas, I.; Fernandez, R.; Gomez-Rodriguez, J.; Colchero, J.; Gomez-Herrero, J.; Baro, A. M. WSXM: A Software for Scanning Probe Microscopy and a Tool for Nanotechnology. *Rev. Sci. Instrum.* **2007**, *78*, No. 013705.